Diagn Interv Radiol 2026; DOI: 10.4274/dir.2026.263831

BREAST IMAGING

ORIGINAL ARTICLE

Comparative analysis of the diagnostic value of dynamic contrast-enhanced magnetic resonance imaging kinetic heterogeneity and apparent diffusion coefficient for grading invasive breast cancer

Xinyu Feng[1]*
Peiwei Ye[2,3]*
Hui Chen[1]
Changyu Liu[1]
Qingqiang Zhu[1]

[1]Northern Jiangsu People's Hospital Affiliated to Yangzhou University, Department of Medical Imaging, Yangzhou, China

[2]Ruijin Hospital, Shanghai Jiaotong University School of Medicine, Department of Radiation Oncology, Shanghai, China

[3]Shanghai Key Laboratory of Proton-Therapy, Shanghai, China

PURPOSE

To quantitatively compare the diagnostic value of dynamic contrast-enhanced (DCE) magnetic resonance imaging (MRI) kinetic heterogeneity and conventional diffusion-weighted imaging (DWI) for the extent of breast cancer infiltration.

METHODS

This study employed a retrospective analysis of DCE-MRI data of patients with invasive breast cancer (IBC) diagnosed by pathology in our hospital between January 2023 and February 2025. The aim was to obtain quantitative measures of kinetic heterogeneity and apparent diffusion coefficients (ADCs) from DWI, and to extract the six main parameters for lesion heterogeneity analysis from preoperative MRI data using MATLAB, SPM12, and R 4.4.1. The parameters included peak, enhancement volume, persistent fraction, plateau, washout, and heterogeneity. The diagnostic efficacy of DCE-MRI, conventional DWI, and their combination on the extent of IBC infiltration was compared by analyzing the receiver operating characteristic curves, sensitivities, specificities, and correlations among the parameters.

RESULTS

The high-grade group exhibited significantly higher peak, plateau, washout, and heterogeneity values, along with lower persistent and ADC values, compared with the low-grade group (all $P < 0.001$); tumor volume did not differ between groups ($P = 0.314$). ADC and persistent fractions were negatively correlated with pathological grade, whereas peak, plateau, washout, and heterogeneity were positively correlated. Receiver operating characteristic analysis showed that heterogeneity achieved a significantly higher area under the curve (AUC) than ADC [0.910, 95% confidence interval (CI): 0.857–0.948 vs. 0.808, 95% CI: 0.741–0.863; DeLong Z = 2.626, $P = 0.009$]. The AUC for the combined model of heterogeneity, peak value, and ADC was 0.969 (95% CI: 0.946–0.992), with a sensitivity of 95.5% and a specificity of 89.2%.

CONCLUSION

DCE-MRI combined with DWI has significant diagnostic value in identifying the extent of IBC infiltration.

CLINICAL SIGNIFICANCE

DCE-MRI kinetic heterogeneity combined with DWI enables noninvasive discrimination of the extent of IBC infiltration before surgery, facilitating personalized systemic therapy and nodal evaluation while avoiding overtreatment in patients at low risk. Computer-aided, whole-tumor heterogeneity analysis replaces limited region-of-interest sampling, significantly improving both efficiency and accuracy of IBC grading. Integration of kinetic heterogeneity plus diffusion parameters provides a panoramic view of tumor size, location, and perilesional relationships, empowering multidisciplinary teams to rapidly individualize surgical and adjuvant treatment strategies.

KEYWORDS

Invasive breast cancer, dynamic contrast-enhanced magnetic resonance imaging, kinetic heterogeneity, diffusion-weighted imaging, apparent diffusion coefficient

***Contributed equally to this work.**

Handling editor: Serap Gültekin

Corresponding author: Qingqiang Zhu

E-mail: zhuqingqiang1983@163.com

Received 25 December 2025; revision requested 11 January 2026; accepted 05 February 2026.

Epub: 26.02.2026

Publication date: 01.07.2026

DOI: 10.4274/dir.2026.263831

You may cite this article as: Feng X, Ye P, Chen H, Liu C, Zhu Q. Comparative analysis of the diagnostic value of dynamic contrast-enhanced magnetic resonance imaging kinetic heterogeneity and apparent diffusion coefficient for grading invasive breast cancer. *Diagn Interv Radiol*. 2026;32(4):399-408.

Invasive breast cancer (IBC) accounts for 70%–80%[1] of breast cancers and poses an elevated recurrence risk due to stromal/vascular infiltration.[2] Accurate preoperative grading is essential for personalized therapy.[3] However, core biopsy—the reference standard—is invasive and limited by sampling error and inter-observer variability.[4,5] Multiparametric magnetic resonance imaging (MRI) offers a non-invasive alternative. Diffusion-weighted imaging (DWI) quantifies cellularity via apparent diffusion coefficient (ADC) values,[6] whereas dynamic contrast-enhanced MRI (DCE-MRI) extracts quantitative parameters based on the pharmacokinetic model of the contrast agent to reveal the perfusion and permeability characteristics of tumor microvessels.[7] Although these techniques reliably differentiate benign from malignant lesions,[8,9] their further application to breast cancer grading remains limited. This is because most studies rely on manual, single-layer region-of-interest (ROI) localization, thereby overlooking spatial heterogeneity.[10] Therefore, it is vital to systematically validate the value of DWI and DCE-MRI quantitative parameters in evaluating the degree of IBC infiltration across an entire tumor scale.

Main points

- High-grade invasive breast cancer (IBC) exhibited significantly higher peak, plateau, washout, and heterogeneity values than low-grade IBC. Conversely, high-grade IBC demonstrated lower persistent fraction and apparent diffusion coefficient values, with no discernible difference in volume values between the two groups.
- Apparent diffusion coefficient, persistent fraction, and IBC grading exhibited a negative correlation. Peak, plateau, washout, and heterogeneity demonstrated a positive correlation with IBC grading. However, no significant correlation was observed between enhancement volume and IBC grading.
- Dynamic contrast-enhanced magnetic resonance imaging kinetic heterogeneity combined with diffusion-weighted imaging has significant diagnostic value in identifying the extent of IBC infiltration.

Computer-aided diagnosis (CAD) overcomes this limitation by enabling voxel-wise quantification of entire tumors, capturing intratumoural heterogeneity from hemorrhage, necrosis, and microvascular variation.[11-13] Previous studies have shown that a stronger washout effect and higher kinetic heterogeneity on DCE-MRI can effectively distinguish benign from malignant breast lesions, reflecting increased angiogenesis and the degree of vascular leakage within the tumor.[14] Additionally, the CAD system automatically detects lesions, thereby reducing interpretation time and substantially lowering the false-positive rate below specific thresholds.[15] Building on these observations, the present study compares whole-tumor ADC and DCE-MRI quantitative parameters in terms of low- and high-grade IBC, evaluating their diagnostic efficacy.

Methods

Patients

This retrospective study analyzed clinical and imaging data from patients with breast cancer admitted to Northern Jiangsu People's Hospital between January 2023 and February 2025. A total of 203 patients were included (Figure 1). The inclusion criteria were as follows: 1) complete MRI data, including DWI and DCE-MRI; 2) postoperative pathological confirmation of IBC with defined invasive grade; and 3) no prior history of breast cancer surgery, neoadjuvant chemotherapy, or related interventions documented before the imaging examination. The exclusion criteria included 1) poor MRI image quality (e.g., significant artifacts), 2) non-lump cases and other types of breast malignancies, 3) factors impeding accurate image interpretation (including location in special anatomical sites, indistinct lesion boundaries, and lesion size < 5 mm), and 4) pregnancy. The grade of IBC infiltration was classified according to the Nottingham Combined Histological Grading system,[16] an amended version of the Schaff-Blum-Richardson system. IBC was classified into three grades based on ductal formation, nuclear

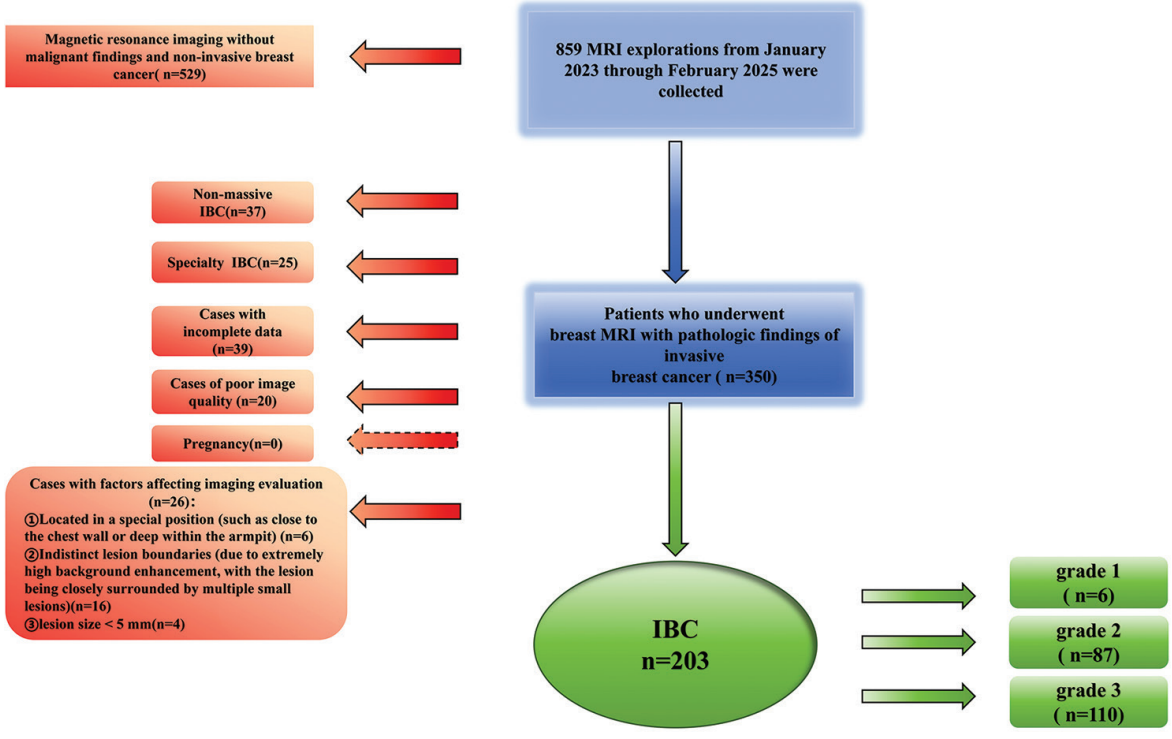

Figure 1. Flowchart showing the patient recruitment process. MRI, magnetic resonance imaging; IBC, invasive breast cancer.

pleomorphism, and mitotic count. According to prior studies, Grades I and II are grouped as low-grade IBC, and Grade III as high-grade IBC.[17] Immunohistochemistry (IHC) was performed using the streptavidin–biotin method to detect estrogen receptor (ER), progesterone receptor (PR), human epidermal growth factor receptor 2 (HER2), and Ki-67 proliferation. HER2 expression status was further confirmed via fluorescence *in situ* hybridization (FISH). If the HER2 IHC result is 3+, it is classified as HER2-positive; if the result is 1+ or 0, it is classified as HER2-negative; if the result is 2+, FISH testing is required to determine the HER2 status.[18] ER and PR positivity is defined as ≥ 1% of tumor cell nuclei showing positive staining. The Ki-67 index is categorized as low proliferation (< 14%) or high proliferation (≥ 14%) based on a cut-off of 14%.[19] This study was approved by the Review Committee of Northern Jiangsu People's Hospital (approval number: 2024ky379, date: December 24, 2024). Informed consent was waived due to the study's retrospective design.

Imaging acquisition

This study utilized the GE Healthcare Discovery MR750W 3.0 T (GE Healthcare, Chicago, IL, USA) MRI system for scanning. Patients were placed in the prone position, with both breasts naturally suspended within a dedicated eight-channel breast phased-array coil. The scan coverage included both breasts, the anterior chest wall, and the axillary regions. The imaging protocol commenced with a localization sequence, followed by axial fat-suppressed T2-weighted turbo spin-echo (TSE) imaging. DCE-MRI images were acquired using a three-dimensional T1-weighted fast gradient echo (LAVA/FLEX) sequence, comprising one pre-contrast and five post-contrast images. Following the pre-contrast acquisition, gadolinium diethyltripropionate (Omniscan, GE Healthcare) was bolus-injected at a flow rate of 2.5 mL/s via the antecubital vein using a high-pressure syringe, at a dose of 0.1 mmol/kg body weight. This was immediately followed by a 20-mL saline flush at the same flow rate. Following scan completion, images were uploaded to the GE Advantage Workstation for routine time-intensity curve (TIC) plotting of lesions. Prior to DCE-MRI, axial fat-suppressed single-shot echo-planar (SS-EPI) DWI was performed. Diffusion gradients were sequentially applied in three orthogonal directions, with an acquisition time of 222 s and b values of 0 and 1,000 s/mm^2. All sequences were acquired axially. Conventional T1-weighted imaging (WI) employed a TSE readout, with repetition time (TR): 4.4 ms, echo time (TE): 2.1 ms, flip angle: 15°, field of view (FOV): 320 × 320 mm^2, phase matrix: 320 × 320, and slice thickness: 1.3 mm. DCE T1-WI used an identical TSE readout, with TR: 5.9 ms, TE: 1.1 ms, flip angle: 15°, FOV: 320 × 320 mm^2, phase matrix: 240 × 240, and slice thickness: 1.3 mm. Fat-suppressed T2-WI was acquired using TR: 4,619 ms, TE: 85 ms, flip angle: 15°, FOV: 320 × 320 mm^2, phase matrix: 224 × 320, and slice thickness: 4 mm. DWI used an SS-EPI sequence in an oblique plane, with TR: 2,859 ms, TE: 88.5 ms, FOV: 320 × 320 mm^2, phase matrix: 128 × 128, and slice thickness: 10 mm.

Image analysis

The DCE-MRI processing workflow was as follows. First, motion correction was performed on all phases of the DCE-MRI images using SPM 12 software, with the criteria that translational and rotational motion were < 1 mm and < 5°, respectively. The corrected images were then imported into ITK-SNAP software (version 3.8.0). Two radiologists (with 5 and 10 years of breast MRI experience, respectively) manually delineated the volume of interest (VOI) on second-phase DCE-MRI images acquired within 120 s of contrast agent injection to maximize lesion-background contrast and enhance delineation consistency.[20,21] Finally, MATLAB (version 2021a) was used to extract DCE parameters within the VOI. The parameters included peak, which is the maximum enhancement ratio (MER) within the tumor between the early peak enhancement phase (120 s post-contrast injection) and the pre-enhanced image. The MER calculation formula is as follows:[22]

$$MER=\frac{S_{peak}-S_{baseline}}{S_{baseline}}\times 100\%,$$

where $S_{baseline}$ = mean signal intensity of the first two pre-contrast phases, and Speak = maximum post-contrast signal intensity per voxel at 120 s.

Further parameters included the following. Enhancement volume, defined as the volume fraction of voxels within the tumor showing over 50% enhancement in the early peak enhancement phase compared with the pre-enhanced image. Persistent fraction, defined in terms of a > 10%-increase in voxel volume in the final phase compared with the early peak enhancement phase in terms of signal intensity. Plateau proportion, where the increase or decrease in the signal intensity ratio between the final phase and the early peak enhancement phase does not exceed 10% in the voxel volume. Washout proportion, defined as a decrease in voxel volume by more than 10% in the final phase compared with the early peak enhancement phase in terms of signal intensity. Heterogeneity, which is a measure of tumor heterogeneity based on the proportion of voxels exhibiting washout, plateau, or sustained enhancement. The formula for the calculation of heterogeneity is as follows:[23]

$$\text{heterogeneity}=-\sum_{i=1}^{k} Pi\log_k Pi$$

where Pi is the frequency of observations of each variable and k is the number of kinetic-class categories; here k: 3 (washout, plateau, persistent). The index ranges from 0 to 1, with higher values indicating greater heterogeneity.[24]

The DWI processing workflow was as follows: DWI data were converted to NIfTI format using MRIcron (https://www.nitrc.org/projects/mricron), then processed using the NeuDiLab software developed based on DIPY (https://dipy.org/). For conventional DWI, the quantitative metric ADC is generated via single-exponent fitting using the following formula:[25]

$$S(b) / S(0) = \exp(-b \cdot ADC),$$

where S(0) and S(b) represent the signal intensity of water molecule motion in the absence and presence of diffusion, respectively; b is the diffusion-sensitization factor determining the degree of diffusion weighting in signal intensity. To measure diffusion metrics, the VOI defined on DCE-MRI was used as a reference. This VOI was placed on the quantitative map of conventional DWI (i.e., ADC), positioned along the tumor margin with the largest dimension, and excluded adjacent normal breast and fatty tissue.

Statistical analysis

All statistical analyses were performed using SPSS 25.0 (IBM Corp., Armonk, NY, USA), MedCalc 19.6 (MedCalc Software, Ostend, Belgium) and R 4.4.1 software (R Foundation for Statistical Computing, Vienna, Austria). Inter-reader reproducibility for continuous parameters was quantified using the intraclass correlation coefficient (ICC), with values > 0.75 indicating excellent agreement. Normality was first examined using the Shapiro–Wilk test. Continuous variables were expressed as mean ± standard deviation if normally distributed, and compared using the independent-sample t-test; otherwise, they were expressed as median (interquartile range) and compared using the Mann–Whitney U test.

To compare the distributions of categorical variables between two groups, the chi-square (χ^2) test was used. When data in the contingency table were sparse—specifically, when more than 20% of expected cell counts were < 5 or any expected count was < 1—the Fisher–Freeman–Halton test (i.e., Fisher's exact test for R × C contingency tables) was used to obtain more reliable and precise *P* values. Univariate logistic regression was used to select initial parameters. Subsequently, a forward stepwise multivariable logistic regression analysis was performed on parameters with $P < 0.05$ to identify the simplest, clinically significant model for distinguishing low-grade from high-grade IBC. The optimal probability threshold for the combined diagnostic model was determined by maximizing Youden's index (J = Sensitivity + Specificity − 1) on the receiver operating characteristic (ROC) curve. To assess the risk of overfitting, stratified bootstrap resampling was used to assess area under the curve (AUC) sampling fluctuations, and the validated average AUC and its 95% confidence interval (CI) were calculated. The calibration curve was used to evaluate the consistency between the model's predicted and observed probabilities. Correlation analyses were performed using Pearson's r for normally distributed continuous variables and Spearman's ρ for non-normally distributed data. Two-tailed *P* values < 0.05 were considered statistically significant.

Results

A total of 203 patients with pathologically confirmed IBC were included (Table 1). Among them, 93 patients (45.8%) were classified as low grade (Grade I, n = 6; Grade II, n = 87), and 110 (54.2%) as high grade. No significant difference was observed in the maximum tumor diameter (29.7 ± 23.0 vs. 24.4 ± 13.8 mm; $P = 0.585$) or PR expression between the low-grade and high-grade groups, whereas statistically significant differences were noted in ER and HER2 expression, and Ki-67 proliferation index ($P < 0.05$). TICs differed significantly between groups ($P = 0.010$): type III curves were more frequent in high-grade IBC (73.6% vs. 53.8%), whereas type I curves predominated in low-grade lesions (7.5% vs. 2.7%). The mean age was similar between the low-grade and high-grade groups (53 ± 10 vs. 55 ± 11 years, $P = 0.053$).

Inter-reader agreement for all quantitative metrics was excellent (ICC > 0.75, $P < 0.05$) (Table 2). High-grade IBC exhibited significantly higher peak enhancement (17.486 ± 23.881 vs. 7.025 ± 5.924, $P < 0.001$), plateau fraction (0.318 ± 0.182 vs. 0.137 ± 0.118, $P < 0.001$), washout fraction (0.210 ± 0.170 vs. 0.105 ± 0.146, $P = 0.007$), and kinetic heterogeneity (0.908 ± 0.191 vs. 0.493 ± 0.239, $P < 0.001$) than low-grade tumors (Table 1, Figure 2). Conversely, the persistent fraction (0.493 ± 0.239 vs. 0.729 ± 0.251, $P < 0.001$) and ADC value (0.770 ± 0.161 vs. 1.010 ± 0.221 × 10^{-3} mm^2/s, $P < 0.001$) were significantly lower in high-grade lesions. No between-group difference in lesion volume was observed ($P = 0.314$). Univariable logistic regression identified peak, persistent, plateau, washout, and heterogeneity as significant predictors of grading IBC ($P < 0.05$) (Table 3). These variables were subsequently entered into a forward stepwise multivariable logistic regression analysis. The final model identified kinetic heterogeneity [odds ratio

Table 1. General data characteristics, DCE-MRI kinetic analysis of each parameter and ADC values of patients with low-grade IBC vs. high-grade IBC

	Low-grade IBC (n = 93)	High-grade IBC (n = 110)	*P*
Age	53 ± 10	55 ± 11	0.053
Tumor length diameter (mm)	29.68 ± 22.99	24.41 ± 13.78	0.585
ER			
+	67	48	< 0.001
–	26	62	
PR			
+	55	53	0.116
–	38	57	
HER2			
+	76	39	< 0.001
–	17	71	
Ki-67			
>14%	46	72	0.018
≤14%	47	38	
TIC			
I	7 (7.53%)	3 (2.73%)	
II	36 (38.71%)	26 (23.64%)	0.010
III	50 (53.76%)	81 (73.63%)	
Peak	7.025 ± 5.924	17.486 ± 23.881	< 0.001
Volume	2,455.591 ± 5,343.670	4,852.045 ± 24,164.594	0.314
Persistent	0.729 ± 0.251	0.493 ± 0.239	< 0.001
Plateau	0.137 ± 0.118	0.318 ± 0.182	< 0.001
Washout	0.105 ± 0.146	0.210 ± 0.170	0.007
Heterogeneity	0.493 ± 0.239	0.908 ± 0.191	< 0.001
ADC	1.010 ± 0.221	0.770 ± 0.161	< 0.001

IBC, invasive breast cancer; ADC, apparent diffusion coefficient; TIC, time-intensity curve; HER2, human epidermal growth factor receptor 2; ER, estrogen receptor; PR, progesterone receptor; DCE, dynamic contrast-enhanced; MRI, magnetic resonance imaging.

Table 2. ICC values for each parameter of DCE-MRI kinetic analysis and ADC values between two observers

Parameters	Two observer ICC values	*P*
Heterogeneity	0.957 (0.935–0.971)	< 0.001
ADC	0.901 (0.883–0.926)	< 0.001
Peak	0.978 (0.928–0.968)	< 0.001
Volume	0.902 (0.837–0.928)	< 0.001
Persistent	0.912 (0.849–0.935)	< 0.001
Plateau	0.900 (0.835–0.925)	< 0.001
Washout	0.961 (0.930–0.970)	< 0.001

ADC, apparent diffusion coefficient; ICC, intraclass correlation coefficient; DCE, dynamic contrast-enhanced; MRI, magnetic resonance imaging.

(OR): 2.500; 95% CI: 1.848–3.373; $P < 0.001$] and peak (OR: 1.130; 95% CI: 1.026–1.244; $P = 0.012$) as independent positive predictors of high-grade IBC, whereas ADC was an independent negative predictor (OR: 0.318; 95% CI: 0.198–0.514; $P < 0.001$) (Figure 3).

The ROC analysis demonstrated good discriminatory power for all quantitative metrics (Figure 4). The AUC values were as follows: peak: 0.680 (95% CI: 0.611–0.744), persistent: 0.765 (95% CI: 0.700–0.821), plateau: 0.806 (95% CI: 0.744–0.858), washout: 0.717 (95% CI: 0.650–0.778), heterogeneity 0.914 (95% CI: 0.866–0.949), and ADC 0.819 (95% CI: 0.758–0.869) (Table 4). Corresponding sensitivities were 55.5%, 69.0%, 65.3%, 64.5%, 86.4%, and 90.3%, with specificities of 78.5%, 79.0%, 87.3%, 74.2%, 84.9%, and 53.6%, respectively. The combined model incorporating heterogeneity, peak, and ADC achieved a sensitivity of 95.5% and a specificity of 89.2% at the optimal threshold of 0.346. DeLong testing revealed that heterogeneity achieved a significantly higher AUC than ADC (0.914 vs. 0.819; $P = 0.009$). In evaluating the generalization ability and overfitting risk of the combined heterogeneity, peak, and ADC comprehensive diagnostic model, the average AUC obtained through stratified bootstrap resampling was 0.969 (95% CI: 0.933–0.985), which was significantly better than that of any single parameter. The calibration curve was plotted based on the final model (Figure 5). The predicted probabilities for each risk group were generally close to the ideal 45° reference line in the overall distribution, indicating acceptable calibration performance.

Correlation analyses were summarized and visualized using a heat map of Pearson coefficients (Figure 6). ADC and persistent fraction were negatively correlated with histological grade (r: −0.533, $P < 0.001$ and r: −0.414, $P < 0.001$, respectively), whereas peak, plateau, washout, and heterogeneity showed positive correlations (r: 0.279, $P < 0.001$; r: 0.505, $P < 0.001$; r: 0.314, $P < 0.001$; and r: 0.695, $P < 0.001$). No significant association was observed between enhancement volume and grade (r: 0.066, $P = 0.350$). Heterogeneity possessed the strongest correlation with invasive status, and the combination of heterogeneity plus ADC yielded the highest diagnostic performance.

Discussion

This study demonstrated that high-grade IBC is characterized by significantly higher peak, plateau, and washout ratios on DCE-MRI, as well as greater heterogeneity, alongside lower persistent fraction ratios and ADC values. The combined diagnostic model incorporating heterogeneity, peak, and ADC achieved an AUC of 0.969, which was significantly superior to that of any single parameter. These findings indicate that combining DCE-MRI with DWI enables quantitative assessment of IBC grading. This approach can provide objective evidence to support

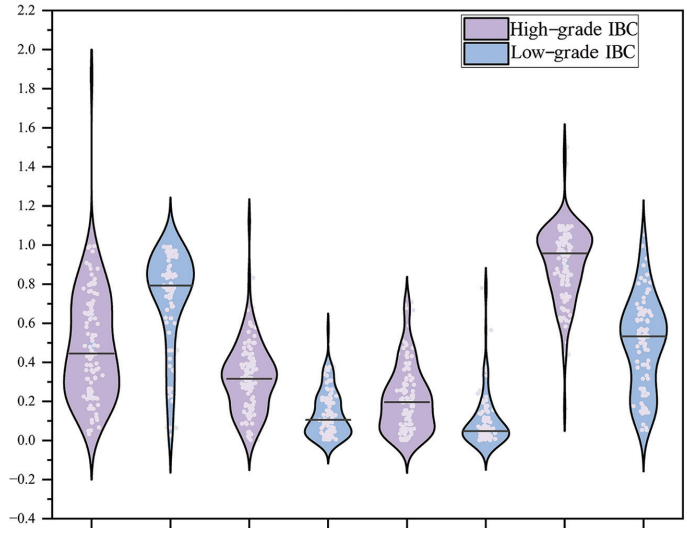

Figure 2. Violin graphs showing the differences in dynamic contrast-enhanced magnetic resonance imaging kinetic parameters and apparent diffusion coefficient values between low-grade and high-grade invasive breast cancer. IBC, invasive breast cancer.

Table 3. Univariable and multivariable logistic regression analyses of the relationship between low-grade and high-grade IBCs

Parameters	Unit change	Univariable			Multivariable		
		OR	95%CI	*P*	OR	95% CI	*P*
ADC	0.1	0.427	0.328–1.000	< 0.001	0.318	0.198–0.514	< 0.001
Heterogeneity	0.1	2.365	1.883–2.971	< 0.001	2.500	1.848–3.373	< 0.001
Peak	1	1.087	1.041–1.135	< 0.001	1.130	1.026–1.244	0.012
Persistent	1	0.035	0.011–0.116	< 0.001			
Plateau	1	4,615.207	369.461–57,651.9451	< 0.001			
Washout	1	113.895	12.249–1,058.998	< 0.001			

ADC, apparent diffusion coefficient; OR, odds ratio; CI, confidence interval; IBC, invasive breast cancer.

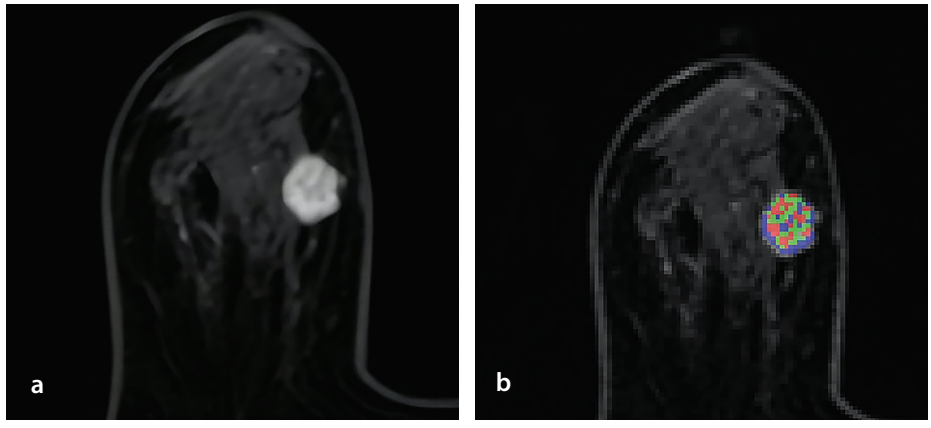

Figure 3. A 46-year-old female with a malignant tumor (high-grade IBC). BI-RADS:5. Dynamic contrast-enhanced kinetic analysis plot (**a** and **b**), peak: 5.983, persistent: 0.430, plateau: 0.312, washout: 0.257, and heterogeneity: 1.075. The blue, green, and red denote persistent, plateau, and washout, respectively. IBC, invasive breast cancer.

precise histological grading and guide individualized treatment planning and axillary management, thereby helping to avoid overtreatment in patients at low risk.

In agreement with the report by Li et al.,[26] which found that high-grade lesions exhibit elevated quantitative parameters, we observed significantly greater kinetic heterogeneity in high-grade IBC than in low-grade tumors (0.908 ± 0.191 vs. 0.493 ± 0.239, $P < 0.001$). Breast cancer heterogeneity is usually accompanied by regional hypoxia and microvascular abnormalities, including disorganized vessel architecture and increased permeability. We therefore postulated that greater kinetic heterogeneity reflects a more complex vascular network and more pronounced histopathological heterogeneity within the tumor microenvironment. Previous studies have demonstrated that tumor infiltration extent is associated with tumor cell growth rate, invasiveness to surrounding tissues, drug sensitivity, and treatment outcomes. Therefore, preoperative grading is of considerable importance in guiding treatment planning.[27] Conversely, ADC values were significantly lower in high-grade IBC than in the low-grade group (0.770 ± 0.161 vs. 1.010 ± 0.221 × 10^{-3} mm^2/s, $P < 0.001$) and showed a strong inverse correlation with invasive grade (r: −0.533, $P < 0.001$), which is in agreement with the findings of Mori et al.[28] This difference is likely attributable to the characteristic pathological features of high-grade tumors, such as marked nuclear pleomorphism, a high mitotic index, and densely packed tumor cells. Spearman correlation analysis further revealed that both ADC and persistent fraction were negatively correlated with histological grade (r: −0.533 and r: −0.414, respectively; $P < 0.001$). This indicates that increased cellular density and reduced sustained perfusion are associated with greater aggressiveness. In contrast, peak, plateau, washout, and heterogeneity were positively correlated with grade (r: 0.279, 0.505, 0.314, and 0.695, respectively; all $P < 0.001$), suggesting that greater perfusion heterogeneity and washout are indicative of higher malignant potential. In this study, the persistent, plateau, and washout parameters were represented by blue, green, and red, respectively. Compared with histogram analysis, which captures overall heterogeneity but

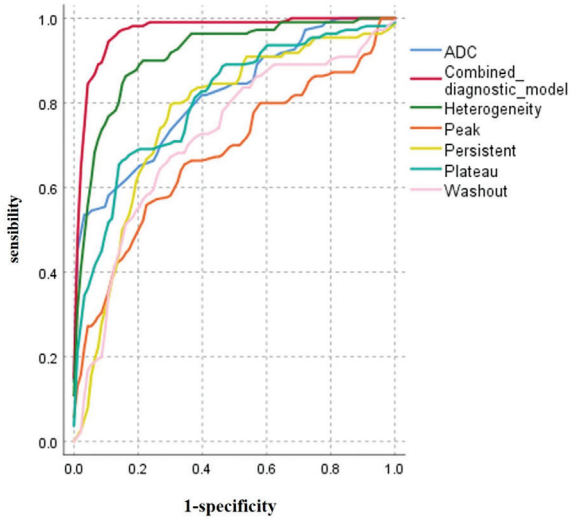

Figure 4. Receiver operating characteristic curve analysis for invasive breast cancer grade identification yielded an area under the curve of 0.910 (95% CI: 0.857–0.948) for heterogeneity, 0.808 (95% CI: 0.741–0.863) for apparent diffusion coefficient, and 0.969 (95% CI: 0.927–0.984) for the combined diagnostic model, demonstrating the superior discriminative performance of the combined model in assessing breast cancer invasiveness. ADC, apparent diffusion coefficient; CI, confidence interval.

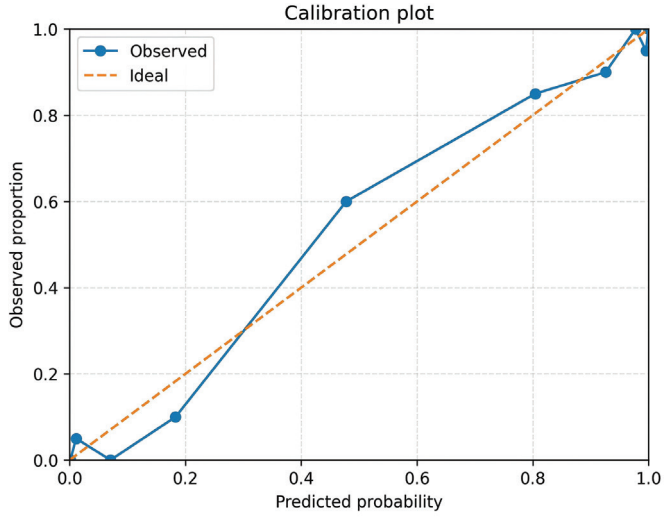

Figure 5. Calibration plot of the final multivariable model. The plot shows that the predicted probabilities across risk groups were generally close to the ideal 45° line, indicating acceptable calibration performance.

Table 4. Comparison of the diagnostic efficacy of DCE-MRI kinetic analysis of each parameter and ADC values between low-grade and high-grade IBCs

Parameters	AUC	95% CI	Sensitivity	Specificity	Cut-off value	Youden index
ADC	0.819	0.758–0.869	90.30%	53.60%	0.735	0.525
Heterogeneity	0.914	0.866–0.949	86.40%	84.90%	0.709	0.713
Peak	0.68	0.611–0.744	55.50%	78.50%	10.322	0.340
Persistent	0.765	0.700–0.821	69.00%	79.00%	0.721	0.499
Plateau	0.806	0.744–0.858	65.30%	87.30%	0.263	0.524
Washout	0.717	0.650–0.778	64.50%	74.20%	0.122	0.387
Combined diagnostic model	0.969	0.946–0.992	95.50%	89.20%	0.346	0.847

ADC, apparent diffusion coefficient; AUC, area under the curve; CI, confidence interval; DCE, dynamic contrast-enhanced; MRI, magnetic resonance imaging; IBC, invasive breast cancer.

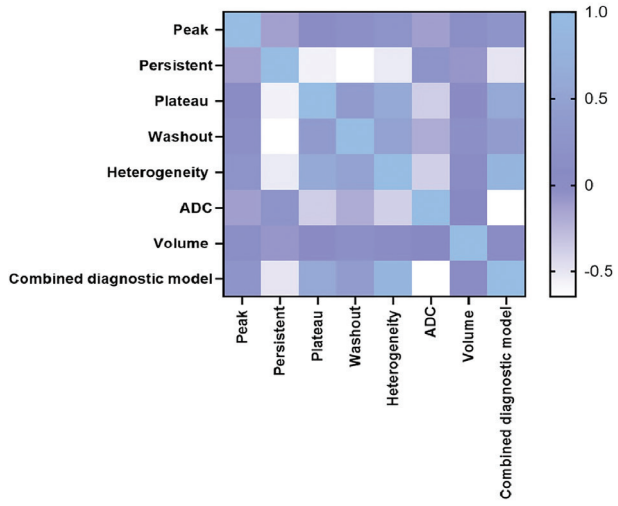

Figure 6. Heatmap of correlations among various parameters of dynamic contrast-enhanced magnetic resonance imaging kinetic analysis, apparent diffusion coefficient (ADC) values, and invasive breast cancer staging; ADC was negatively correlated with histological grade (r: –0.533, $P < 0.001$), whereas heterogeneity showed positive correlations (r: 0.695, $P < 0.001$).

loses spatial information, the core advantage of our model lies in preserving the spatial distribution map of heterogeneity. This enables us to identify and localize specific subregions within tumors that may represent the highest invasive potential or potential therapeutic resistance, which holds potential significance for guiding targeted biopsy or localized dose-fractionation radiotherapy.

This study is consistent with previous reports that combined DWI and DCE-MRI to improve the estimation of pathological grade in breast cancer.[29,30] The present study focused exclusively on invasive carcinoma of no special type (NST), the most common histological subtype, to eliminate biological heterogeneity among subtypes.[31] DCE-MRI combined with DWI technology has been applied in the preoperative evaluation of breast cancer to assess tumor size and internal structure. DCE imaging can demonstrate the extent of tumor lesions, providing reliable references for surgical planning. However, it is important to note that approximately 10%–15% of all IBCs, specifically invasive lobular carcinomas (ILCs),[32-36] exhibit delayed peak enhancement and infrequent contrast washout on DCE-MRI,[37] markedly differing from the rapid enhancement pattern seen in NST. The biological basis of ILC may relate to its diffuse growth pattern and reduced neovascularization requirements, manifested by lower vascular endothelial growth factor levels and more mature, low-permeability tumor vasculature,[38-40] resulting in overall weaker enhancement. Given the potential limitations of traditional assessment parameters for lesions with atypical enhancement patterns, the heterogeneity index used in this study quantifies voxel-level perfusion gradients to reflect spatial heterogeneity in microvascular function. Theoretically less dependent on lesion enhancement intensity or sharp margins, this index is hypothesized to retain discriminatory potential for ILC, although its value requires further validation through subgroup analysis. Fan et al.[41] constructed radiomic signatures from single-phase DCE-MRI and ADC maps, achieving AUCs of 0.811 and 0.816 for tumor grading, respectively; both values are significantly lower than the AUC of 0.969 obtained with the combined model of heterogeneity, peak, and ADC. A probable explanation is that static radiomics extracts thousands of features from a limited cohort, yielding features with questionable biological interpretability, whereas our kinetic heterogeneity metric quantifies time-resolved hypoxia and microvascular abnormalities across all perfusion phases, thereby providing complementary information to radiomics approaches. It should be noted that although this study demonstrates superior technical-level discriminative efficacy compared with conventional methods and attempts to provide biologically interpretable features, it remains within the scope of retrospective technical validation. Whether it can ultimately influence surgical decisions, assist in treatment selection, or improve patient outcomes requires validation in prospective clinical settings.

In the present study, high-grade IBC exhibited a significantly higher peak than low-grade tumors (17.486 ± 23.881 vs. 7.025 ± 5.924, $P < 0.001$), a finding consistent with previous work,[42] which demonstrated a strong association between greater peak enhancement and higher histological grade and advanced clinical stage. Peak enhancement reflects the early increase in signal intensity after contrast injection and thus mirrors the concentration of contrast medium in the intravascular and extravascular compartments.[43] We therefore postulate that the elevated peak in high-grade lesions is closely linked to altered tumor microvasculature. In this study of low-grade IBC, we found that 53.8% of cases exhibited a type III TIC, whereas previous similar studies reported approximately 34% of breast cancers presenting a type II TIC.[44] Furthermore, existing research indicates that distinguishing benign from malignant breast lesions often requires reliance on the most suspicious TIC classification,[45] suggesting that TIC generation is highly dependent on the ROI delineated by the operator. If the ROI is not accurately placed within the rapidly enhancing washout region, it may compromise the curve's representativeness and thus interfere with diagnostic judgment.[46] Therefore, precise ROI localization is critical for the reliability of diagnostic accuracy. However, this study overcomes the errors associated with manual placement through whole-tumor quantitative analysis, with results indicating that the proportion of persistent IBC was significantly higher in low-grade IBC than in high-grade IBC (0.729 ± 0.251 vs. 0.493 ± 0.239, $P < 0.001$), whereas the proportion of plateau-stage IBC was significantly lower in low-grade IBC than in high-grade IBC (0.137 ± 0.118 vs. 0.318 ± 0.182, $P < 0.001$). These findings indicate that high-grade IBC exhibits a marked reduction in persistent fraction and a corresponding increase in plateau. Consequently, the persistent and plateau parameters demonstrate potential utility in the graded diagnosis of IBC, offering crucial evidence for distinguishing low-grade from high-grade IBC. Research[47] has suggested that plateau may reflect the distribution and proportion of invasive tumor cells within breast cancer, presenting novel insights for noninvasive diagnosis; however, further clinical validation is required.

Immunohistochemical analysis in this study further revealed statistically significant differences in HER2 expression status and Ki-67 proliferation index across different histological grades, consistent with previous findings.[48,49] Prior studies have demonstrated that high Ki-67 proliferation correlates with aggressive growth and higher tumor grades in breast cancer, with tumor cell proliferation

often exhibiting spatially heterogeneous distribution.[50] Recent studies have utilized multiparametric MRI for noninvasive assessment of the biological characteristics of breast cancer.[51,52] This suggests that integrating complementary imaging and pathological information is crucial for developing predictive models that comprehensively interpret tumor heterogeneity, providing important insights for further refinement of this research. Additionally, although some early studies have reported a correlation between tumor volume and histological grade,[53] our analysis found no significant association between manually segmented tumor volume and grade ($P = 0.314$). This finding aligns with data from large-scale population studies. For example, in an analysis of 161,708 breast cancers from the SEER Program, Schwartz et al.[54] found that tumor size accounted for < 10% of the variance in histological grade. Notably, 15%–20% of tumors smaller than 1 cm were classified as Grade III, indicating that small lesions can be biologically aggressive. Similarly, Liu et al.[16] reported no correlation between invasive tumor size and any DCE-MRI perfusion parameter (all $P > 0.05$), and Schmitz et al.[55] found no association between macroscopic diameter and micro-vessel density on 3.0 T breast MRI. Collectively, these data suggest that invasive potential is driven more by intrinsic biological traits, such as angiogenic activity, cellular density, and genomic instability, than by physical tumor bulk. Furthermore, our volume segmentation deliberately excluded peritumoural edema, a methodological choice that may have reduced any incidental correlation between edema-rich large lesions and high-grade disease. Based on this evidence, we hypothesize that tumor size is not a determinant of angiogenic factors or blood perfusion in IBC.

Our study has several limitations. First, this was a single-center, exploratory study with a relatively small sample size. The model coefficients and calibration have not been verified in external cohorts, and the potential risk of overfitting cannot be completely ruled out. Second, this study was restricted to patients with NST lesions who had not received any breast cancer-related treatment, which may limit the generalizability of kinetic parameters to other IBC subtypes and introduce selection bias. Future research will further evaluate the diagnostic efficacy of DCE-MRI and DWI in assessing the response to neoadjuvant therapy. Third, tumor VOIs were manually delineated, introducing inter-observer variability. Artificial intelligence-based auto-segmentation should be explored to improve reproducibility and efficiency. Finally, heterogeneity analysis was performed using MATLAB and SPM12; inter-institutional differences in acquisition protocols and software packages hinder feature harmonization. Future work should establish standardized imaging protocols and consensus analysis pipelines to enhance the clinical portability of kinetic biomarkers.

In conclusion, this study employed volumetric quantitative DCE-MRI enhancement classification technology to visualize and quantitatively analyze the kinetic heterogeneity within tumors. Combined with ADC values, the model's diagnostic efficacy in evaluating IBC grades surpassed that of a single parameter. This provides a new and promising imaging biomarker for noninvasive assessment of tumor heterogeneity, although its exact clinical application value needs to be verified through subsequent prospective studies.

Footnotes

Conflict of interest disclosure

The authors declared no conflicts of interest.

References

1. Yang WT, Bu H. [updates in the 5(th) edition of WHO classification of tumours of the breast]. *Zhonghua Bing Li Xue Za Zhi*. 2020;49(5):400-405. [Crossref]
2. Facina G, Oliveira VMD. Breast cancer care during the coronavirus pandemic. *Mastology*. 2020;30. [Crossref]
3. Wang J, Wu SG. Breast cancer: An overview of current therapeutic strategies, challenge, and perspectives. *Breast Cancer (Dove Med Press)*. 2023;15:721-730. [Crossref]
4. Wang W, Dou B, Wang Q, et al. Comparison of MUSE-DWI and conventional DWI in the application of invasive breast cancer and malignancy grade prediction: a comparative study. *Heliyon*. 2024;10(2):e24379. [Crossref]
5. Rakha EA, El-Sayed ME, Menon S, Green AR, Lee AH, Ellis IO. Histologic grading is an independent prognostic factor in invasive lobular carcinoma of the breast. *Breast Cancer Res Treat*. 2008;111(1):121-127. [Crossref]
6. Zhu G, Dong Y, Zhu R, et al. Dynamic contrast-enhanced magnetic resonance imaging parameters combined with diffusion-weighted imaging for discriminating malignant lesions, molecular subtypes, and pathological grades in invasive ductal carcinoma patients. *PLoS One*. 2025;20(4):e0320240. [Crossref]
7. Zhang D, Shen M, Zhang L, He X, Huang X. Establishment of an interpretable MRI radiomics-based machine learning model capable of predicting axillary lymph node metastasis in invasive breast cancer. *Sci Rep*. 2025;15(1):26030. [Crossref]
8. Gullo RL, Partridge SC, Shin HJ, Thakur SB, Pinker K. Update on DWI for breast cancer diagnosis and treatment monitoring. *AJR Am J Roentgenol*. 2024;222(1):e2329933. [Crossref]
9. Morris EA, Liberman L, Ballon DJ, et al. MRI of occult breast carcinoma in a high-risk population. *AJR Am J Roentgenol*. 2003;181(3):619-626. [Crossref]
10. Mann RM, Cho N, Moy L. Breast MRI: State of the Art. *Radiology*. 2019;292(3):520-536. [Crossref]
11. Junttila MR, De Sauvage FJ. Influence of tumour micro-environment heterogeneity on therapeutic response. *Nature*. 2013;501(7467):346-354. [Crossref]
12. Gerlinger M, Rowan AJ, Horswell S, et al. Intratumour heterogeneity and branched evolution revealed by multiregion sequencing. *N Engl J Med*. 2012;366(10):883-892. [Crossref] Erratum in: *N Engl J Med*. 2012;367(10):976.
13. Kim C, Suh JY, Heo C, et al. Spatiotemporal heterogeneity of tumour vasculature during tumour growth and antiangiogenic treatment: MRI assessment using permeability and blood volume parameters. *Cancer Med*. 2018;7(8):3921-3934. [Crossref]
14. Yao Y, Mou F, Kong J, Liu X. Kinetic heterogeneity improves the specificity of dynamic enhanced MRI in differentiating benign and malignant breast tumours. *Acad Radiol*. 2024;31(3):812-821. [Crossref]
15. Lehman CD, Peacock S, DeMartini WB, Chen X. A new automated software system to evaluate breast MR examinations: Improved specificity without decreased sensitivity. *AJR Am J Roentgenol*. 2006;187(1):51-56. [Crossref]
16. Liu L, Mei N, Yin B, Peng W. Correlation of DCE-MRI perfusion parameters and molecular biology of breast infiltrating ductal carcinoma. *Front Oncol*. 2021;11:561735. [Crossref]
17. Takahashi H, Oshi M, Asaoka M, Yan L, Endo I, Takabe K. Molecular biological features of nottingham histological grade 3 breast cancers. *Ann Surg Oncol*. 2020;27(11):4475-4485. [Crossref]
18. Wolff AC, Hammond ME, Hicks DG, et al. Recommendations for human epidermal growth factor receptor 2 testing in breast cancer: American Society of Clinical Oncology/College of American Pathologists clinical practice guideline update. *Arch Pathol Lab Med*. 2014;138(2):241-256. [Crossref]
19. Nielsen TO, Leung SCY, Rimm DL, et al. Assessment of Ki67 in Breast Cancer: Updated Recommendations From the International Ki67 in Breast Cancer Working Group. *J Natl Cancer Inst*. 2021;113(7):808-819. [Crossref]

20. Hu N, Zhao J, Li Y, et al. Breast cancer and background parenchymal enhancement at breast magnetic resonance imaging: A meta-analysis. *BMC Med Imaging*. 2021;21(1):32. [Crossref]
21. Giannotti E, James JJ, Chen Y, et al. Effectiveness of percutaneous vacuum-assisted excision (VAE) of breast lesions of uncertain malignant potential (B3 lesions) as an alternative to open surgical biopsy. *Eur Radiol*. 2021;31(12):9540-9547. [Crossref] Erratum in: *Eur Radiol*. 2022;32(1):742. [Crossref]
22. Kuhl CK, Mielcareck P, Klaschik S, et al. Dynamic breast MR imaging: Are signal intensity time course data useful for differential diagnosis of enhancing lesions? *Radiology*. 1999;211(1):101-110. [Crossref]
23. Kim JY, Kim JJ, Hwangbo L, et al. Kinetic heterogeneity of breast cancer determined using computer-aided diagnosis of preoperative MRI scans: relationship to distant metastasis-free survival. *Radiology*. 2020;295(3):517-526. [Crossref]
24. Zhao R, Ma WJ, Tang J, et al. Heterogeneity of enhancement kinetics in dynamic contrast-enhanced MRI and implication of distant metastasis in invasive breast cancer. *Clin Radiol*. 2020;75(12):961. [Crossref]
25. Mao C, Hu L, Jiang W, et al. Discrimination between human epidermal growth factor receptor 2 (HER2)-low-expressing and HER2-overexpressing breast cancers: a comparative study of four MRI diffusion models. *Eur Radiol*. 2024;34(4):2546-2559. [Crossref]
26. Li K, Machireddy A, Tudorica A, et al. Discrimination of malignant and benign breast lesions using quantitative multiparametric MRI: a preliminary study. *Tomography*. 2020;6(2):148-159. [Crossref]
27. Allarakha A, Gao Y, Jiang H, Wang PJ. Prediction and prognosis of biologically aggressive breast cancers by the combination of DWI/DCE-MRI and immunohistochemical tumor markers. *Discov Med*. 2019;27(146):7-15. [Crossref]
28. Mori N, Inoue C, Tamura H, et al. Apparent diffusion coefficient and intravoxel incoherent motion-diffusion kurtosis model parameters in invasive breast cancer: correlation with the histological parameters of whole-slide imaging. *Magn Reson Imaging*. 2022;90:53-60. [Crossref]
29. Goldhirsch A, Winer EP, Coates AS, et al. Personalizing the treatment of women with early breast cancer: Highlights of the st gallen international expert consensus on the primary therapy of early breast cancer 2013. *Ann Oncol*. 2013;24(9):2206-2223. [Crossref]
30. Fan M, Yuan C, Huang G, et al. A framework for deep multitask learning with multiparametric magnetic resonance imaging for the joint prediction of histological characteristics in breast cancer. *IEEE J Biomed Health Inform*. 2022;26(8):3884-3895. [Crossref]
31. Jeong J, Park CS, Lee JW, et al. Computer-aided diagnosis parameters of invasive carcinoma of no special type on 3T MRI: correlation with pathologic immunohistochemical markers. *J Korean Soc Radiol*. 2022;83(1):149-162. [Crossref]
32. Parvaiz MA, Yang P, Razia E, et al. Breast MRI in invasive lobular carcinoma: a useful investigation in surgical planning? *Breast J*. 2016;22(2):143-150. [Crossref]
33. Hussien M, Lioe TF, Finnegan J, Spence RA. Surgical treatment for invasive lobular carcinoma of the breast. *Breast*. 2003;12(1):23-35. [Crossref]
34. Li CI, Anderson BO, Daling JR, Moe RE. Trends in incidence rates of invasive lobular and ductal breast carcinoma. *JAMA*. 2003;289(11):1421-1424. [Crossref]
35. Peiro G, Bornstein BA, Connolly JL, et al. The influence of infiltrating lobular carcinoma on the outcome of patients treated with breast-conserving surgery and radiation therapy. *Breast Cancer Res Treat*. 2000;59(1):49-54. [Crossref]
36. Li CI, Daling JR. Changes in breast cancer incidence rates in the United States by histologic subtype and race/ethnicity, 1995 to 2004. *Cancer Epidemiol Biomarkers Prev*. 2007;16(12):2773-2780. [Crossref]
37. Mann RM, Hoogeveen YL, Blickman JG, Boetes C. MRI compared to conventional diagnostic work-up in the detection and evaluation of invasive lobular carcinoma of the breast: a review of existing literature. *Breast Cancer Res Treat*. 2008;107(1):1-14. [Crossref]
38. Arpino G, Bardou VJ, Clark GM, Elledge RM. Infiltrating lobular carcinoma of the breast: tumor characteristics and clinical outcome. *Breast Cancer Res*. 2004;6(3):R149-156. [Crossref]
39. Korhonen T, Huhtala H, Holli K. A comparison of the biological and clinical features of invasive lobular and ductal carcinomas of the breast. *Breast Cancer Res Treat*. 2004;85(1):23-29. [Crossref]
40. Molland JG, Donnellan M, Janu NC, Carmalt HL, Kennedy CW, Gillett DJ. Infiltrating lobular carcinoma--a comparison of diagnosis, management and outcome with infiltrating duct carcinoma. *Breast*. 2004;13(5):389-396. [Crossref]
41. Fan M, Yuan W, Zhao W, et al. Joint prediction of breast cancer histological grade and ki-67 expression level based on DCE-MRI and DWI radiomics. *IEEE J Biomed Health Inform*. 2020;24(6):1632-1642. [Crossref]
42. Nam SY, Ko ES, Lim Y, et al. Preoperative dynamic breast magnetic resonance imaging kinetic features using computer-aided diagnosis: Association with survival outcome and tumor aggressiveness in patients with invasive breast cancer. *PLoS One*. 2018;13(4):e0195756. [Crossref]
43. Tofts PS, Brix G, Buckley DL, et al. Estimating kinetic parameters from dynamic contrast-enhanced t1-weighted MRI of a diffusable tracer: standardized quantities and symbols. *J Magn Reson Imaging*. 1999;10(3):223-232. [Crossref]
44. Dietzel M, Zoubi R, Vag T, et al. Association between survival in patients with primary invasive breast cancer and computer aided MRI. *J Magn Reson Imaging*. 2013;37(1):146-155. [Crossref]
45. Cho N, Kim SM, Park JS, et al. Contralateral lesions detected by preoperative MRI in patients with recently diagnosed breast cancer: application of MR CAD in differentiation of benign and malignant lesions. *Eur J Radiol*. 2012;81(7):1520-1526. [Crossref]
46. Piccoli CW. Contrast-enhanced breast MRI: factors affecting sensitivity and specificity. *Eur Radiol*. 1997;7(Suppl 5):281-288. [Crossref]
47. Baltzer PAT, Zoubi R, Burmeister HP, et al. Computer assisted analysis of MR-mammography reveals association between contrast enhancement and occurrence of distant metastasis. *Technol Cancer Res Treat*. 2012;11(6):553-560. [Crossref]
48. El-Hawary AK, Abbas AS, Elsayed AA, Zalata KR. Molecular subtypes of breast carcinoma in Egyptian women: clinicopathological features. *Pathol Res Pract*. 2012;208(7):382-386. [Crossref]
49. Li J, Chen Z, Su K, Zeng J. Clinicopathological classification and traditional prognostic indicators of breast cancer. *Int J Clin Exp Pathol*. 2015;8(7):8500-8505. [Crossref]
50. Coates AS, Winer EP, Goldhirsch A, Gelber RD, Gnant M, Piccart-Gebhart M, Thürlimann B, Senn HJ; Panel Members. Tailoring therapies--improving the management of early breast cancer: St Gallen International Expert Consensus on the Primary Therapy of Early Breast Cancer 2015. *Ann Oncol*. 2015;26(8):1533-1546. [Crossref]
51. Yuan C, Jin F, Guo X, Zhao S, Li W, Guo H. Correlation Analysis of breast cancer DWI combined with DCE-MRI imaging features with molecular subtypes and prognostic factors. *J Med Syst*. 2019;43(4):83. [Crossref]
52. Cao M, Liu X, Yang A, Xu Y, Zhang Q, Cao Y. Prediction of HER-2 expression status in breast cancer based on multi-parameter MRI intratumoral and peritumoral radiomics. *Magn Reson Imaging*. 2025;122:110434. [Crossref]
53. Chen ST, Lai HW, Tseng HS, Chen LS, Kuo SJ, Chen DR. Correlation of histologic grade with other clinicopathological parameters, intrinsic subtype, and patients' clinical outcome

in Taiwanese women. *Jpn J Clin Oncol*. 2011;41(12):1327-1335. [Crossref]

54. Schwartz AM, Henson DE, Chen D, Rajamarthandan S. Histologic grade remains a prognostic factor for breast cancer regardless of the number of positive lymph nodes and tumor size: a study of 161 708 cases of breast cancer from the SEER Program. *Arch Pathol Lab Med*. 2014;138(8):1048-1052. [Crossref]

55. Schmitz AC, Peters NHGM, Veldhuis WB, et al. Contrast-enhanced 3.0-T breast MRI for characterization of breast lesions: Increased specificity by using vascular maps. *Eur Radio*. 2008;18(2):355-364. [Crossref]